PROCEEDINGS, 46th Workshop on Geothermal Reservoir Engineering
Stanford University, Stanford, California, February 15-17, 2021
SGP-TR-218

An Analysis of the Demonstration of a CO_2-based Thermosiphon at the SECARB Cranfield Site

Benjamin M. Adams[1,2], Mark R. Fleming[2,3], Jeffrey M. Bielicki[4,5], Nagasree Garapati[6,7], and Martin O. Saar[6,1]

[1]Department of Earth and Environmental Sciences, University of Minnesota, Minneapolis, MN, USA
[2]Department of Mechanical Engineering, University of Minnesota, Minneapolis, MN, USA
[3]Department of Mechanical Engineering, Milwaukee School of Engineering, Milwaukee, WI, USA
[4]Department of Civil, Environmental, and Geodetic Engineering, The Ohio State University, Columbus, OH, USA
[5]John Glenn College of Public Affairs, The Ohio State University, Columbus, OH, USA
[6]Geothermal Energy and Geofluids Group, Department of Earth Sciences, ETH-Zurich, Zurich, Switzerland
[7]Department of Chemical and Biomedical Engineering, West Virginia University, Morgantown, WV, USA

adam0068@umn.edu

Keywords: CO_2-geothermal, CO_2-Plume Geothermal (CPG), Thermosiphon, Carbon Capture Utilization and Storage (CCUS)

ABSTRACT

CO_2 Plume Geothermal (CPG) is a CO_2-based geothermal electricity generation system that circulates CO_2 into the geologic reservoir instead of water. When CO_2 is circulated through a deep (> 2 km) sedimentary reservoir, it extracts more heat per unit pumping power than water due to the decreased viscosity of supercritical CO_2. Additionally, the compressibility of CO_2 generates a pressure differential at the surface, allowing electricity to be generated directly from the produced geofluid instead of with an Organic Rankine Cycle. Therefore, CPG has the potential to generate geothermal electricity from reservoirs where water geothermal is uneconomical. However, the steps necessary to develop a CPG pilot depend on the field demonstration of the circulation of geologically stored CO_2 between a sedimentary reservoir and the surface. To date, the CO_2 circulation test at the SEACARB Cranfield site has been the only demonstration. While the test showed that sequestered CO_2 may be re-produced and circulated from the subsurface, the test did not develop a non-zero, steady, thermosiphon-generated recirculation rate, as is expected when CO_2 is used as the subsurface working fluid.

In this paper, we analyze the publicly-available test results for the CO_2 circulation test at the SECARB Cranfield site and describe the underlying physics which produced those results. We employ a numerical wellbore heat loss model to test the effect of wellbore fluid heat loss on the thermosiphon-generated fluid mass flowrate. We find that the accumulation of high-density fluid (i.e., water) within the production wellbore could cause the thermosiphon-generated recirculation flowrate to asymptote to zero, as it did during the field test. Most importantly, we find that a self-sustaining thermosiphon is not necessary for the successful operation of a CO_2-based geothermal system and that the inclusion of a CO_2 injection pump would have allowed for sustained circulation rates regardless of the production well fluid composition.

1. INTRODUCTION

Geothermal electricity generation can provide reliable baseload or dispatchable power generation with few carbon emissions. Unlike wind and solar renewable generation which generate electricity as the resource is available, geothermal energy can provide electricity as needed by the electric grid. Flexible, carbon-neutral electricity generation will be essential to decarbonize the electric grid.

CO_2 Plume Geothermal (CPG) is an electricity generation technology which circulates sequestered CO_2 from a geologic reservoir with the surface, generating electricity (Randolph and Saar, 2011). The CO_2 is likely sequestered in a sedimentary reservoir as part of a mitigation action to combat global climate change, providing 'utilization' of the CO_2. CPG is thus a carbon capture utilization and storage (CCUS) technology. CPG has been found to generate more electricity than water-based geothermal systems in porous reservoirs at moderate temperatures, depths, and permeabilities (Adams et al., 2015).

Using CO_2 as the subsurface working fluid in a CPG system has many advantages, including lower viscosity than water and increased compressibility than water (Adams et al., 2014). The reduced viscosity of the CO_2 leads to lower frictional losses in the subsurface, which decreases the pump work needed to extract heat from the reservoir, making CO_2 a more efficient heat exchange fluid. The density of CO_2 also varies substantially with pressure and temperature (i.e., it has high compressibility), and this has the benefit of inducing a thermosiphon, which aids in the circulation of the CO_2, reducing the need for pumping (Adams et al., 2014). However, a self-sustained thermosiphon is not necessary for CPG operation as CO_2 may still be pumped through the reservoir to extract heat like is already necessary in a water-based geothermal system.

In January 2015, a thermosiphon test was made at the SECARB Cranfield CFU31 CO_2 sequestration site in Cranfield, Mississippi (Freifeld et al, 2016; Pan et al., 2018). The site is operated by the South Eastern Regional Partnership for Carbon Sequestration (SECARB), which had been sequestering approximately 3 kg/s of CO_2 continuously into the CFU 31F-01 injection well as part of a carbon sequestration test since 2009 (Pan et al., 2018). The test unit is located within the Tuscaloosa sand formation, is 3.2 km deep, 23 m thick, has an average reservoir pressure of 32.5 MPa and temperature of 129°C (Pan et al., 2018). Thus, assuming a 10°C surface temperature, the site has a geologic temperature gradient of ~37 °C/km.

The thermosiphon test consisted of two wells: CFU 31F-01 (injection well) and CFU 31F-03 (production well), spaced about 100 m apart at the surface. The two wells were connected via pipeline at the surface with a flowmeter in the pipeline to measure flowrate between injection and production well. A heat exchanger was used prior to reinjection to cool the CO_2 to approximately 12°C, assuring higher density CO_2 in the injection well than the production well. To begin the test, CO_2 was vented from the production well, causing fluid movement up the production well. In a CO_2-based geothermal system, the CO_2 fluid pressure at the surface is substantially more than atmospheric pressure (e.g., ~6 MPa in Adams et al. (2015)), allowing venting to occur. Once CO_2 movement had begun, the production well vent was closed and the CO_2 was instead routed into the injection well. At this point, the system was a closed-loop that was circulating CO_2 to and from the subsurface.

Over three days, the test was performed three times. Each time, the self-circulation mass flowrate was highest immediately after the venting, but then slowly, asymptotically reduced to zero. In the third test, the maximum CO_2 circulation rate was approximately 1 kg/s immediately after venting and non-zero flowrate circulation lasted for at least 40 hours (Pan et al., 2018).

In Adams et al. (2014), we showed that a non-zero CO_2 thermosiphon-generated flowrate would result for reservoir depths greater than 500 m with a 35 °C/km geologic temperature gradient. This thermosiphon-generated flowrate is due to the large difference in CO_2 fluid densities in the injection and production wells. However, in Adams et al. (2014), transient effects during the initiation of circulation were not considered, the fluid was assumed to be pure CO_2, and there was no heat transfer from the wellbore fluid to the surrounding rock. As the result of the Cranfield field test was a zero steady state flowrate, one or more of these assumptions was not valid for the Cranfield site and we investigate the effects of these assumptions.

In this paper, there are two objectives: 1) to explain the asymptotical approach to zero flowrate of the CO_2 thermosiphon at the Cranfield site, and 2) most importantly, to show that a self-sustaining thermosiphon is not necessary for CO_2-based geothermal power systems.

2. METHODOLOGY

First, we explain the theory behind a thermosiphon (Section 2.1). Then, we explain the numeric model used to measure the resulting thermosiphon-generated mass flowrate of the Cranfield site (Section 2.2).

2.1 Thermosiphon Theory

A thermosiphon is a natural, buoyancy-driven flow of fluid. The flow is driven by the pressure difference created by the fluid density difference in injection and production wells.

Figure 1 shows a simple geothermal system. The geologic fluid ascends the well from States 1 to 2, heat is removed at the surface to State 3, the fluid is reinjected to State 4, after which energy is added in the subsurface.

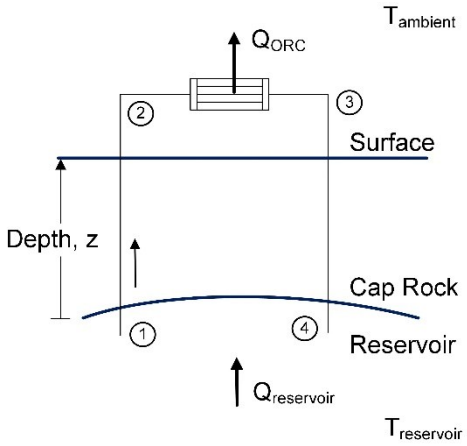

Figure 1: Simple thermosiphon system to explain thermosiphon theory.

In the production well, a fluid energy balance between the entrance (State 1) and exit (State 2) is shown in Equation 1, neglecting the effects of kinetic energy, where h is the enthalpy, z is the depth, and g is the gravitational constant.

$$h_1 + g \cdot z_1 = h_2 + g \cdot z_2 \tag{1}$$

The injection and production wells are fluid compression and expansion processes, respectively. During a fluid expansion or compression process, the work done by the fluid is equal to the change in enthalpy between inlet and exit, less heat losses, shown in Equation 2. In Equation 2, P is the fluid pressure, ρ is the fluid density, η is the isentropic efficiency to account for non-ideal pressure losses within the well, and Q_{loss} is the rock-fluid heat loss (negative if leaving fluid to the rock).

$$\eta \int \frac{dP}{\rho} = \int dh + Q_{loss} \tag{2}$$

Equations 1 and 2 can be combined and evaluated into Equation 3 for the production well, where $\bar{\rho}_p$ is the effective fluid density in the production well, η_p is the production well efficiency, and $Q_{loss,p}$ is the production well heat loss. The effective fluid density is approximately the average density within the well, but is a single value which satisfies Equation 2.

$$\eta_p \frac{P_2 - P_1}{\bar{\rho}_p} = g(z_1 - z_2) + Q_{loss,p} \tag{3}$$

Similarly, Equation 4 shows the energy balance for the injection well, where $\bar{\rho}_i$ is the effective fluid density in the injection well, η_i is the injection well efficiency, and $Q_{loss,i}$ is the injection well heat loss.

$$\eta_i \frac{P_4 - P_3}{\bar{\rho}_i} = g(z_3 - z_4) + Q_{loss,i} \tag{4}$$

In the production well, the fluid enthalpy decreases from inlet to exit and heat is lost from the fluid to the surroundings, thus all of $(h_2 - h_1)$, $(z_1 - z_2)$, and $Q_{loss,p}$ are negative. Similarly, in the injection well, all of $(h_4 - h_3)$, $(z_3 - z_4)$, and $Q_{loss,i}$ are positive. Thus, we can see that all else constant, non-zero heat loss in the production and injection wells will increase the difference between wellbore inlet and exit pressures.

If we assume the injection and production wellhead pressures at the surface are equivalent, we can combine Equations 3 and 4 to yield the difference in pressure across the reservoir, $P_4 - P_1 = \Delta P_{ts}$, where ΔP_{ts} is the thermosiphon-generated pressure difference.

$$\Delta P_{ts} = \frac{\bar{\rho}_i}{\eta_i}\left[g(z_3 - z_4) + Q_{loss,i}\right] + \frac{\bar{\rho}_p}{\eta_p}\left[g(z_1 - z_2) + Q_{loss,p}\right] \tag{5}$$

Assuming that the change in elevation is $\Delta z = (z_3 - z_4)$ and that $z_1 = z_4$ and $z_2 = z_3$, Equation 5 can be rewritten as Equation 6.

$$\Delta P_{ts} = \frac{\bar{\rho}_i}{\eta_i}\left[g \cdot \Delta z + Q_{loss,i}\right] - \frac{\bar{\rho}_p}{\eta_p}\left[g \cdot \Delta z - Q_{loss,p}\right] \tag{6}$$

If the wells are assumed adiabatic ($Q_{loss} = 0$) and isentropic ($\eta = 1$), Equation 6 reduces to Equation 7.

$$\Delta P_{ts} = \left(\bar{\rho}_i - \bar{\rho}_p\right) \cdot g \cdot \Delta z \tag{7}$$

The thermosiphon-generated pressure difference is thus directly proportional to the difference between effective densities of the injection and production wells. This also illustrates why the thermosiphon-generated pressure is so much larger for CO_2 than water—at a 1 km depth, the CO_2 injection and production well effective densities are 860 and 335 kg/m^3, respectively, while the water injection and production well effective densities for the same example are 1149 and 1133 kg/m^3, respectively (Adams et al, 2014, Section 3.1). Thus, the CO_2 density difference is approximately 400 kg/m^3, while the water density difference is approximately 20 kg/m^3.

In this hypothetical example, the thermosiphon-generated mass flowrate only overcomes the reservoir frictional pressure losses. The mass flowrate of the system could be found by solving for the reservoir mass flowrate which produced pressure losses equivalent to the thermosiphon-generated pressure. In a real geothermal system, the thermosiphon-generated pressure difference, ΔP_{ts}, and the additional pump pressure differences, $\Delta P_{pumping}$, reach equilibrium with the sum of the surface, wellbore, and reservoir pressure losses, ΔP_{losses}, shown in Equation 8.

$$\Delta P_{ts} + \Delta P_{pumping} = \Delta P_{losses} \tag{8}$$

The pressure losses in pipes or reservoirs are always a function of mass flowrate, $\dot{m}$, and dependent on other medium-specific parameters, such as pipe diameter, D, or porous media permeability, κ, as shown in Equation 9. The operating mass flowrate thus is determined by the balancing of pressure gains and losses, described in Equation 8.

$$\Delta P_{losses} = f(\dot{m}, D, \kappa, \dots) \tag{9}$$

When non-zero heat losses (i.e., positive $Q_{loss,i}$ and negative $Q_{loss,p}$) are considered in Equation 6, all else constant, the thermosiphon-generated pressure difference, ΔP_{ts}, increases. Thus, we can say that, all else constant, the inclusion of production wellbore heat loss (or injection wellbore heat gain), will increase the thermosiphon-generated pressure difference. This would, in turn, increase the thermosiphon-generated mass flowrate. There is, however, the complicating factor that heat loss will also affect the fluid density.

If non-zero heat losses (i.e., positive $Q_{loss,i}$ and negative $Q_{loss,p}$) are considered in Equation 6, but the effective well fluid densities are varied, a sufficiently high production well effective density (or sufficiently low injection well effective density) can still result in a zero thermosiphon-generated pressure.

Thus, while the inclusion of wellbore heat loss should increase the thermosiphon-generated pressure (and thus the flowrate) for relatively incompressible fluids (i.e., water), it is unclear how it will affect compressible fluids (i.e., CO_2). To evaluate the extend of this effect, a numerical model will have to be made.

2.2 System Model

A numerical model was made to estimate the thermosiphon generated flowrate of a system. This model is identical to the CO_2-based geothermal power cycle of Adams et al. (2015), but with the following modifications:

- The surface turbine has been removed and replaced with a frictionless pipe,
- No pipe losses are considered at the surface,
- The reservoir impedance is fixed at 20 kPa-s/kg,
- The wellbore fluid composition in any element may be as much as 10%, 50%, or 80% water, and
- Heat transfer between the wellbore fluid and surrounding rock is added.

The numerical simulation parameters used are given in Table 1. All other values are adopted from Adams et al. (2015).

Table 1: Simulation Parameters

Parameter	Value
Reservoir Depth	3.2 km
Reservoir Temperature	129°C
Reservoir Pressure	32.5 MPa
Surface Ambient Temperature	10°C
Fluid Reinjection Temperature	10°C
Reservoir Impedance	20 kPa-s/kg
Pipe Diameter	0.061 m
Pump Pressure Difference	2 MPa (first hour) 0 MPa (thereafter)
Pump Efficiency	0.9
Wellbore Water Mass Fraction (X)	= 0% (pure CO_2) or ≤ 10% or ≤ 50% or ≤ 80%
Well Mesh Elements	6 radial: (0.15 m, 0.3 m, 0.5 m, 0.8 m, 1.2 m, 2 m); 32 axial: (100 m length)
Rock Density	2300 kg/m^3
Rock Thermal Conductivity	2.5 W/m-C
Rock Specific Heat	920 J/kg-C

The system modeled is shown in Figure 2. Fluid is produced from the reservoir at State 1. It rises in the production well, losing heat to the surrounding rock, $Q_{production}$, where it is produced at State 2. The fluid is cooled to the ambient temperature, $T_{ambient}$, removing heat $Q_{surface}$, (State 3), optionally pumped 2 MPa during the first hour (State 4), and reinjected into the injection well, where it gains heat from the surrounding rock, $Q_{injection}$. The fluid enters the reservoir at State 5, and the pressure difference between the inlet and exit of the reservoir is determined by the product of the reservoir impedance and fluid mass flowrate. The fluid is heated to the reservoir temperature, $T_{reservoir}$, with heat, $Q_{reservoir}$. As the system has no surface turbine, the fluid pressure is higher than in Adams et al. (2015) and is always supercritical. The system is pumped during the first hour to approximate the venting period at the Cranfield test site.

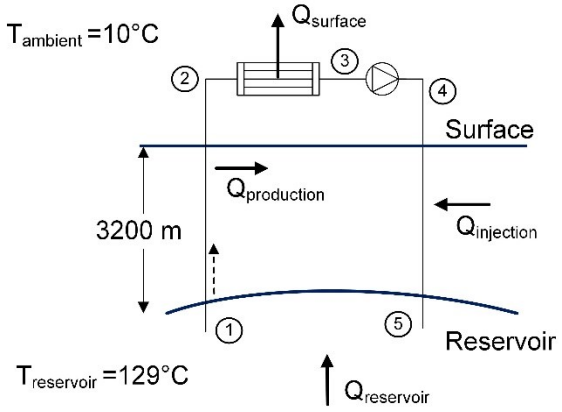

Figure 2: Numerical simulation cycle diagram.

Within the wellbore, the ratio of water mass to total (CO_2 and water) mass is given by the wellbore water mass fraction, X, shown in Equation 10, where m_{water} is the mass of water in a wellbore element and m_{CO2} is the mass of CO_2 in a wellbore element. An assumed wellbore water mass fraction is used as the calculation of the actual value is complex and would require multiphase pipe fluid dynamics simulations.

$$X = \frac{m_{water}}{m_{water}+m_{CO2}} \tag{10}$$

At time zero, the wellbore water mass fraction is zero in all production well elements and the fraction is always zero in the injection well. In the pure-CO_2 case, the production wellbore water mass fraction is always zero. For all other cases, as time progresses, water enters the production well at a rate of 2% of the total mass flowrate into the well. The water accumulates, rather than being produced from the well, filling each element to its allowed maximum wellbore water mass fraction, after which the water begins filling the next-higher element. Eventually, the surface of the water will reach the wellhead.

Within the wellbore model, the element enthalpy and pressure are calculated similarly to Adams et al. (2015), namely using patched Bernoulli (Equation 11) and an energy balance (Equation 12), where P_i is the element pressure, ρ_i is the element density, Δz is the change in elevation, g is the gravitational constant, h_i is the element enthalpy, and $\dot{Q}_{Loss,i}$ is the heat from the fluid element to the surrounding rock. The frictional pressure losses are calculated with the Darcy-Weisbach equation using the CO_2 fluid properties. The element density is the mass-weighted-average bulk density using the wellbore water mass fraction of the element.

$$P_{i+1} = P_i - \rho_i \cdot g \cdot \Delta z - \Delta P_{Loss,i} \tag{11}$$

$$h_{i+1} = h_i - g \cdot \Delta z - \frac{\dot{Q}_{Loss,i}}{\dot{m}} \tag{12}$$

The heat loss from the element, $\dot{Q}_{Loss,i}$, is found using a finite element method and based on the code of Randolph et al. (2012). This code is used out of convenience; more recently, semi-analytic heat transfer solutions have also been used (Adams et al., 2020; submitted). A schematic of the heat transfer model is shown in Figure 3.

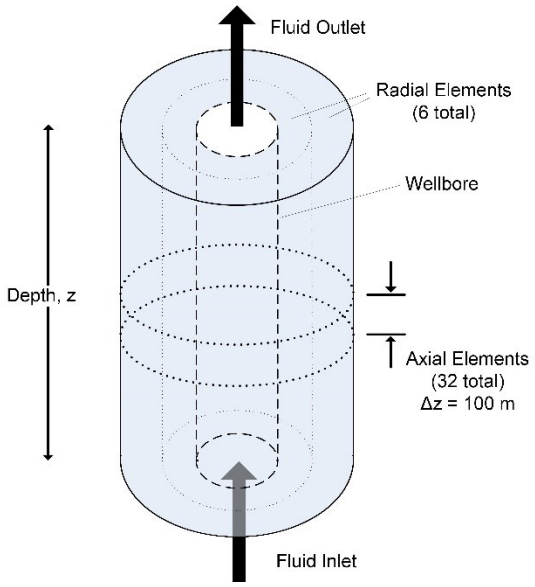

Figure 3: Schematic of finite element heat transfer model used around wellbore.

The heat transfer model is one-dimensional radially, conducting heat between the wellbore fluid and the far-field rock. The far-field rock is at a constant temperature equal to the 10°C surface temperature plus the product of the depth and the 37.1 °C/km temperature gradient. While 32 axial elements were used, heat conduction in rock was not considered between radial elements at different axial positions. For further description of the heat transfer model, see Randolph et al. (2012).

3. RESULTS

First, we present results for a pure CO_2 (no water) case (Section 3.1). Then we present results which show the effect of aggregating water within the production well (Section 3.2). Lastly, we argue that a self-sustaining thermosiphon is not a requirement for CO_2-based geothermal (Section 3.3).

3.1 Pure CO_2 Thermosiphon

In Section 2.1, we showed that the thermosiphon-generated pressure difference by a production and injection well pair is largely a function of the difference between the effective production and injection well fluid densities. Also, we showed that if no pump is used, the resulting mass flowrate of a system is a function of the thermosiphon-generated pressure difference. Thus, the strength (i.e., resulting mass flowrate) of an unpumped thermosiphon is proportional to the difference between production and injection well densities, shown in Equation 13. Therefore, wellbore density plots are made to determine the strength of the thermosiphon.

$$\dot{m} \propto \left(\bar{\rho}_i - \bar{\rho}_p\right) \tag{13}$$

Figure 4 shows the density profiles of the injection and production wells as a function of depth and time. The Figure 4 inset shows the resulting mass flowrate and production wellhead temperature as a function of time. At any given time, the thermosiphon strength (i.e., resulting mass flowrate) can be determined from Figure 4 by the magnitude of difference of density profiles between the two wells.

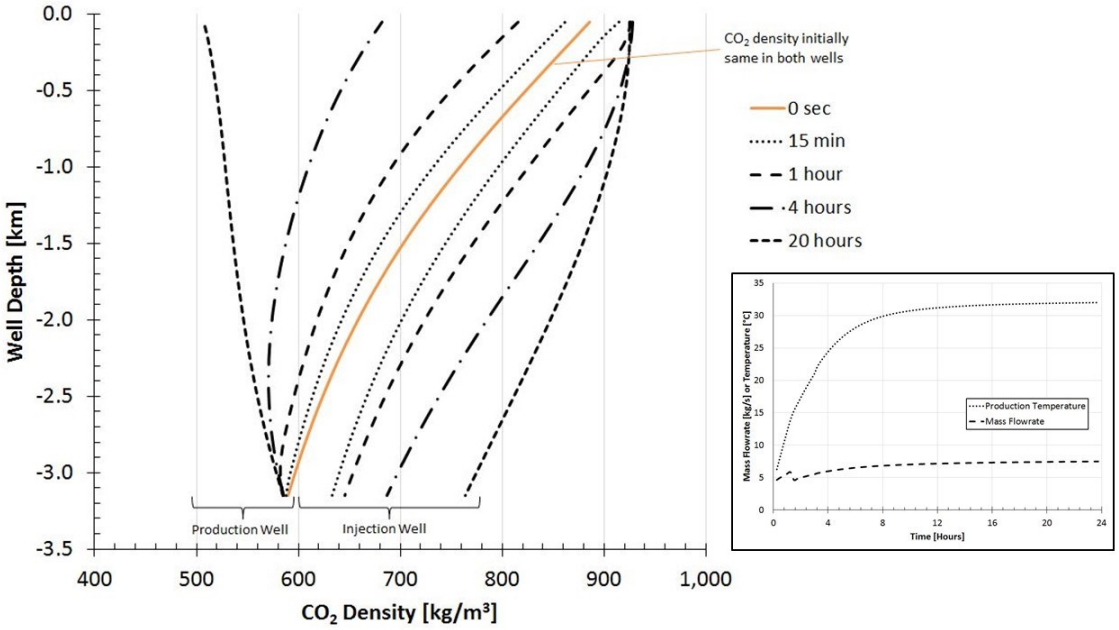

Figure 4: Wellbore CO_2 density profile as a function of time for the pure CO_2 case. Inset: mass flowrate and production wellhead temperature for the first 24 hours.

First, it can be seen that a growing mass flowrate is found for this case, approaching a non-zero asymptote. This is directly attributed to the increasing difference between production and injection wellbore densities with time. The system reaches a quasi-steady state after only about a day of circulation. The asymptotically rising production wellhead temperature similarly shows the increasing temperature, and thus lower density, of the production well CO_2. The wellhead production temperature is substantially lower than the reservoir temperature due to the small flowrate in the production well. At much higher flowrates, above approximately 40 kg/s, the production temperature approaches the reservoir temperature and wellbore heat loss may be neglected (Randolph et al., 2012; Adams et al., submitted). The flowrate may be increased by increasing the well diameter, pumping, or some combination of the both.

At time-zero, the density profiles of both wells are identical as both wells contain static columns of CO_2, with identical temperature profiles which match the geologic temperature gradient. As time progresses, the production well loses less heat to the well surroundings, and the heat flux through the rock-fluid interface diminishes as the surrounding rock increases in temperature. In the same way, the injection well mines heat from the rock surrounding the well, the heat flux diminishes, and the fluid injected into the reservoir decreases in temperature.

Figure 4 also shows that at no depth is the density of CO_2 in the production well greater than the injection well. The closest the two fluids get in density is at time-zero, when they are equal. However, immediately after the onset, the injection well density will increase and the production well density will decrease, due to the heat exchange surrounding the well. As the heat flux continues to decrease into the fluid, the CO_2 density profiles grow increasingly disparate. Thus, it appears that a pure CO_2 thermosiphon is a stable system which naturally

trends towards a non-zero operating mass flowrate. This is evidenced by both the separation of density profiles and the tendency for wellbore heat loss to increase the thermosiphon-generated pressure difference (Equation 5).

Figure 5 shows the heat exchange between the surroundings and the fluid for the four different segments of the fluid circuit: injection well, reservoir, production well, and surface. The specific heat addition is the total heat through the rock-fluid boundary (i.e., kW_{th}) divided by the wellbore mass flowrate (i.e., kg/s). The discontinuity after one hour is due to the cessation of pumping.

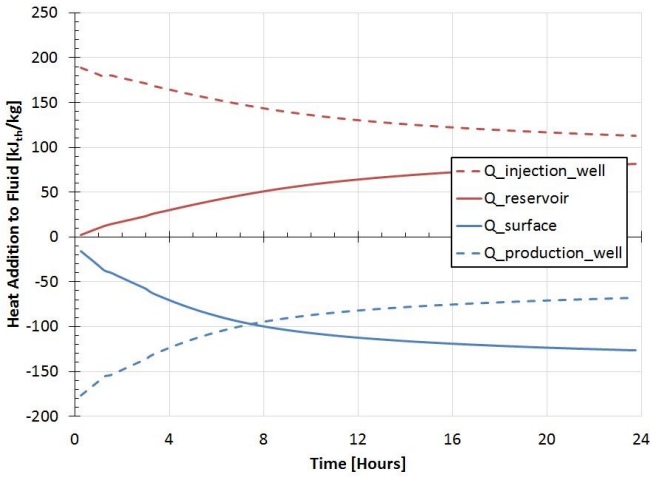

Figure 5: Specific heat addition (positive) or removal (negative) from wellbore CO_2 over time.

Figure 5 shows that at small time, the primary source of heat addition to the fluid (and removal from the fluid) are the wells and not the surface heat exchanger or reservoir. At small time, the production wellhead fluid temperature will by very similar to the surface rock temperature. In this case, little heat is removed using the surface heat exchanger. Similarly, at small time, the fluid arriving at the injection well downhole will be nearly the reservoir temperature, thus little heat is added to the fluid in the reservoir itself.

Figure 5 also shows that the initiation of the thermosiphon is insensitive to the reservoir or surface temperatures—short circuiting within the reservoir will initially not prohibit a thermosiphon from forming, nor will the absence of a sufficiently low heat sink at the surface. Heat to drive the thermosiphon will initially be transferred primarily from the production well to the injection well. Of course, the quality of the heat exchange in the subsurface and the surface are still very important after a few days time.

3.2 Effect of Accumulating Wellbore Water

The previous section showed that a pure CO_2 thermosiphon will tend towards a non-zero steady-state mass flowrate. However, the results of the Cranfield test showed the opposite result, that the system tends towards a mass flowrate of zero. To explain this result, we have included the accumulation of water in the production well in our model. By doing so, we can drive the production well density to greater than the injection well, resulting in a flowrate of zero. Figure 6 shows the mass flowrate and well water level versus time for wellbore water mass fractions of 10%, 50%, and 80%.

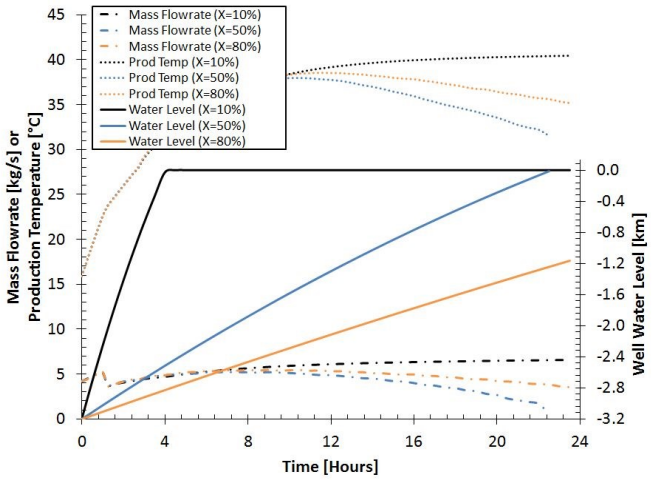

Figure 6: Mass flowrate and production temperature as water accumulates in the well over time.

In all cases, the water flowrate into the production well is 2% of the total mass flowrate; however, when only 10% of the mass in a well element may be water, the water level reaches the surface in only four hours. Conversely, if a large fraction of mass in a well element may be water, the level climbs more slowly. In the case of the low water content (X=10%), the high density of the water does not sufficiently increase the production well bulk density to stop the thermosiphon and the mass flowrate continues to increase with time. Only in the medium (X=50%) and high (X=80%) water content cases is the production well effective density raised sufficiently high that the system mass flowrate begins to decrease. This decrease in mass flowrate causes an accompanying decrease in production wellhead temperature.

Figure 7 shows the wellbore bulk density profiles as a function of depth and time for wellbore water mass fractions of 50% and 80%.

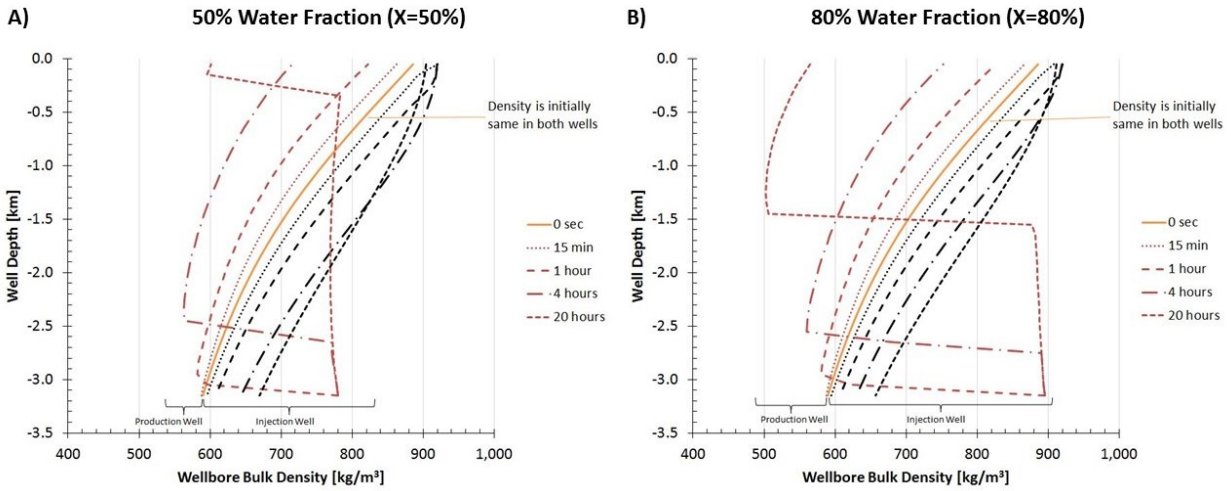

Figure 7: Wellbore density profiles with accumulating water for a wellbore water mass fraction of (A) 50% and (B) 80%.

Both the cases shown in Figure 7 have sufficiently high fluid density in the production well to cause the mass flowrate to inflect in Figure 6. However, only the 80% case is likely to have the mass flowrate converge to zero. Figure 6 shows that at approximately 24 hours time, the 50% case wellbore completely fills with water, but still has a non-zero mass flowrate. As no more water accumulation is possible in this simulation, the mass flowrate will also not decrease further. In fact, though it was not modeled, the reinjection of water into the injection well will cause the injection well density to increase and begin to increase the thermosiphon-generated flowrate once again. Conversely, it appears that after approximately 40 hours time, the production well density line of Figure 7B will have densities greater than the injection well, which would ultimately cause a thermosiphon-driven circulation rate of zero. Thus, we conclude that the thermosiphon-generated mass flowrate of a CO_2-based geothermal system is most likely driven to zero by the presence of large quantities of high-density fluid aggregating in the production well.

3.3 Thermosiphon-generated Flowrate Not Necessary for CO_2-based Geothermal

In the previous sections, we explained the theory behind a thermosiphon generated for a CO_2-based geothermal system and described how high-density bulk fluid in the production well could have driven the thermosiphon-generated flowrate to zero in the Cranfield test.

However, it is important to note that a self-sustaining thermosiphon is not necessary for the successful operation of a CO_2-based geothermal system. Granted, a thermosiphon has long been a selling point for the use of CO_2 as a subsurface geothermal working fluid. However, it is primarily the low viscosity and simplicity of a CO_2 system which provide a benefit over water-based geothermal systems. This explains why a water-based geothermal system generates more electricity at very high transmissivities and most depths than a CO_2-based system (Adams et al., 2020; submitted) When the advantage of small reservoir frictional losses is removed, both the CO_2 and water systems generate similar amounts of electricity. Ultimately, any geothermal system operates on the fundamental principle of extracting heat from the subsurface and bringing it to the surface for use, and this is possible irrespective of the existence of a self-sustaining thermosiphon.

Additionally, Adams et al. (2015) found that additional net power may be generated by pumping the CO_2 to further increase the mass flowrate beyond the flowrate generated by the thermosiphon. Thus, it is likely that any CO_2-based power system will have a pump already included in the system. As pumping can still be used to circulate fluid, no matter the production well fluid density, the working fluid in a CO_2-based geothermal system can still be circulated to generate electricity. Also, it is possible that the fluid produced into the production well will dry-out with time and the full benefit of the CO_2 thermosiphon may be realized.

4. CONCLUSIONS

In this paper, we examined the physics of a thermosiphon and used a numerical model to explain the lack of a self-sustaining thermosiphon during a field test at the Cranfield CO_2 sequestration test site in January 2015. Through our analysis, we can make the following conclusions:

- The thermosiphon-generated mass flowrate is proportional to the difference in fluid densities between the injection and production well.
- Heat transfer between the wellbore fluid and the surrounding rock, instead of an adiabatic well, will cause an increase in the thermosiphon-generated mass flowrate, all else constant.
- A pure CO_2 thermosiphon will tend towards a steady-state, non-zero thermosiphon-generated mass flowrate as the heat transfer through the rock-fluid interface decreases.
- The accumulation of high-density fluid in the production well would cause the decreasing mass flowrate that asymptotically approached zero during the Cranfield tests. Further, in our simulations, only a wellbore filled with an 80% water mass fraction showed potential to decrease the thermosiphon-generated mass flowrate to zero. The 10% and 50% cases only showed a reduction in the non-zero, steady state mass flowrate achieved.
- A self-sustaining thermosiphon is not necessary for the successful operation of a CO_2-based geothermal system. In the event of water accumulation in the production well, the system may be pumped to circulate the hot geologic fluid to the surface, just like a water-based geothermal system.

ACKNOWLEDGEMENTS

Funding from a National Science Foundation (NSF) Sustainable Energy Pathways (SEP) Program Grant (1230691) is gratefully acknowledged. The Werner Siemens Foundation (Werner Siemens-Stiftung) is further thanked for its support of the Geothermal Energy and Geofluids (GEG.ethz.ch) Group at ETH Zurich. We also thank the U.S. National Science Foundation Innovations at the Nexus of Food, Energy, and Water Systems (INFEWS) program (1739909), the U.S. National Science Foundation National Research Traineeship Program (1922666), and the Sloan Foundation. Any opinions, findings, conclusions, and/or recommendations expressed in this material are those of the authors and do not necessarily reflect the views of the UMN, ETH, MSOE, WVU, or The Ohio State University.

REFERENCES

Adams, B.M., Kuehn, T.H., Bielicki, J.M., Randolph, J.B., & Saar, M.O. (2014). On the importance of the thermosiphon effect in CPG (CO_2 plume geothermal) power systems. *Energy*, 69, 409-418. http://dx.doi.org/10.1016/j.energy.2014.03.032

Adams, B.M., Kuehn, T.H., Bielicki, J.M., Randolph, J.B., & Saar, M.O. (2015). A comparison of electric power output of CO_2 Plume Geothermal (CPG) and brine geothermal systems for varying reservoir conditions. *Applied Energy*, 140, 365-377. https://doi.org/10.1016/j.apenergy.2014.11.043

Adams, B.M., Saar, M.O., Bielicki, J.M., Ogland-Hand, J.D., & Fleming, M.R. (2020). Using geologically sequestered CO_2 to generate and store geothermal electricity: CO_2 Plume Geothermal (CPG). *Proceedings of MIT A+B Applied Energy Symposium*, 12-14 Aug, 2020. https://doi.org/10.3929/ethz-b-000444911

Adams, B.M., Ogland-hand, J.D., Bielicki, J.M., Schädle, P., & Saar, M.O. (submitted). Estimating the geothermal electricity generation potential of sedimentary basins using genGEO (the generalizable GEOthermal techno-economic simulator*). Energy & Environmental Science*. preprint: https://doi.org/10.26434/chemrxiv.13514440.v1

Doughty, D. & Freifeld, B.M. (2013). Modeling CO_2 injection at Cranfield, Mississippi: Investigation of methane and temperature effects. *Greenhouse Gas Science Technology*, 3, 475-490. https://doi.org/10.1002/ghg.1363

Freifeld, B.M., Pan, L., Doughty, C., Zakem, S., Hart, K., & Hostler, S. (2016). Demonstration of Geothermal Energy Production Using Carbon Dioxide as a Working Fluid at the SECARB Cranfield Site, Cranfield, Mississippi. *PROCEEDINGS, 41st Workshop on Geothermal Reservoir Engineering Stanford University*, Stanford, California, February 22-24, 2016.

Pan, L., Doughty, C., & Freifeld, B. (2018). How to sustain a CO_2-thermosiphon in a partially saturated geothermal reservoir: Lessons learned from field experiment and numerical modeling. *Geothermics*, 71, 273-293. https://doi.org/10.1016/j.geothermics.2017.10.004

Randolph, J.B. & Saar, M.O. (2011). Combining geothermal energy capture with geologic carbon dioxide sequestration. *Geophysical Research Letters*, 38, L10401. https://dx.doi.org/10.1029/2011GL047265

Randolph, J.B., Adams, B.M., Kuehn, T.H., & Saar, M.O. (2012). Wellbore heat transfer in CO_2-based geothermal systems. *Geothermal Resources Council Transactions*, 36, 549-554.